JOURNAL OF SPACECRAFT AND ROCKETS
Vol. 48, No. 4, July–August 2011

Intersatellite Separation Mechanism for the JC2Sat Formation-Flying Mission

Casey Lambert* and Alfred Ng†
Canadian Space Agency, St. Hubert, Quebec J3Y 8Y9, Canada
and
Yosuke Nakamura‡ and Hiroshi Horiguchi§
Japan Aerospace Exploration Agency, Tsukuba, 305-8505, Japan

DOI: 10.2514/1.51896

There is significant potential for reducing spacecraft complexity and cost by distributing functions and instruments among several smaller spacecraft. As the individual spacecraft's propulsive capabilities inevitably decrease with size, the on-orbit separation behavior becomes a more critical stage of the mission. The intersatellite separation dynamics for a nanosatellite formation-flying mission are investigated using simplified linear relationships for a circular reference orbit. The dynamics performance in terms of collision avoidance, along-track drift, and cross-track periodic motion are assessed to define the separation requirements to achieve the objectives of the JC2Sat mission, which include formation-flying using only differential drag. To accomplish the low-speed separation required for this mission a new type of separation mechanism was developed. This device was ground-tested using pendulum-supported masses. The tests revealed an excess of strain energy stored in the satellite structure that prevents the desired low-speed separation. A simple design modification was made to limit the energy transfer, and a low-speed separation was demonstrated.

Nomenclature

A = cross-sectional area of spacecraft, m^2
a = semimajor axis of elliptical orbit, km
C_D = drag coefficient
d = horizontal distance during pendulum test, m
e = orbit eccentricity
F = input force, N
g = acceleration due to gravity, m/s^2
i = inclination angle of orbit, deg
J_2 = coefficient of first zonal gravitational perturbation
l = length of pendulum support wire, m
m = mass of spacecraft, kg
N = number of orbits
n = mean motion, rad/s
p = semiparameter of elliptical orbit
R_E = radius of Earth, km
r = radius of orbit, km
t = time, s
$\mathbf{V_0}$ = separation velocity, cm/s
v = speed, m/s
x = relative position in radial direction of Hill's frame, m
y = relative position in along-track direction of Hill's frame, m
z = relative position in cross-track direction of Hill's frame, m
α = elevation angle of separation, deg
β = azimuth angle of separation, deg
θ = angle of plane change during separation, deg
μ = gravitational parameter, km^3/s^2
ρ = atmospheric density, kg/m^3
Ω = right ascension of the ascending node, deg

I. Introduction

SIGNIFICANT progress has been made in recent years toward the miniaturization of space technology, which has led to new classes of spacecraft that lower cost and risk, thereby enabling many new players to develop, launch, and operate space assets. Fleeter [1] coined the term *microspace* to describe this emerging area of small-scale spacecraft development. Despite the rapid pace of small-scale satellites reaching orbit, the inherent limit on payload size has thus far prevented comprehensive space missions at this scale. However, this does not preclude that meaningful and relatively significant missions are not currently being conducted with small-scale satellites.

One promising approach to exploit the benefits of miniature satellites is to simply multiply their numbers and, when possible, distribute a payload among a cluster of spacecraft flying in formation. There are numerous technical challenges with this approach related to relative navigation, intersatellite communication, formation control [2], micropropulsion, and distributed instrument technology, but the current work focuses exclusively on the problem of intersatellite separation. The requirements for separating small satellites either from the launch vehicle, the primary payload, or from each other are likely to be more stringent than for conventional satellites because of their small mass and the limited propulsive resources available onboard. Also, because of their nominal relegation as a secondary or piggyback payload, small satellites are often prohibited from using pyrotechnical devices to achieve separation. Therefore, a thorough understanding of the dynamics of separation is required, as well as a reliable device or mechanism to accomplish the desired separation while respecting strict launch guidelines.

It is clear that the miniaturization of formation-flying spacecraft is best served by the absence of a propulsion system, which may be possible by generating relative accelerations using differential aerodynamic drag techniques [3–5], electromagnetic manipulation [6], or solar radiation pressure [7,8]. However, for most small-scale formation-flying missions such as PRISMA [9] (which was launched in June 2010) or the CanX-4 and CanX-5 missions (which are

Presented as Paper 2010-7957 at the AIAA/AAS Astrodynamics Specialist Conference, Toronto, Canada; received 5 August 2010; revision received 29 March 2011; accepted for publication 29 March 2011.

*Natural Science and Engineering Research Council Visiting Fellow, Engineering Development. Member AIAA.
†Manager, Control Group, Engineering Development. Member AIAA.
‡Associate Senior Engineer, Space Technology Demonstration Research Center.
§Manager, Space Technology Demonstration Research Center.

currently under development [10,11]), the spacecraft is equipped with a classical propulsion system.

The focus of this work is the low-speed separation dynamics and the intersatellite separation mechanism (ISM) for the Japan Canada Joint Collaboration Satellites (JC2Sat) project, which is a nanosatellite formation-flying demonstration mission that relies solely on differential drag [4,12]. Specific details of the JC2Sat mission are presented in Sec. II. Although the separation dynamics analysis and the ISM development and testing are centered on this specific mission, the results may be applicable to many small-scale formation-flying missions and also certain conventional formation-flying applications.

Most studies on the performance of formation-flying spacecraft commence with convenient initial conditions for relative position and velocity [2–8,12,13]. The question of how the spacecraft reached these respective orbits is often neglected, despite the potential challenges posed. This work assumes that the two spacecraft in a leader–follower or chief–deputy configuration initially reach orbit together, and separation occurs when an equal-and-opposite force is experienced. The dynamics behavior following this separation is studied in terms of the ability of the spacecraft to attain the desired formation, as opposed to the traditional approach of assuming ideal initial conditions. There are three distinct aspects of the separation dynamics that are part of this analysis: collision avoidance, drift-stop distance, and cross-track motion. Each must be carefully considered in the determination of the desired separation speed and direction. For formation-flying spacecraft with little or no propulsive resources, this understanding of the intersatellite separation dynamics is critical.

Although intersatellite separation on orbit is becoming a more common occurrence, specific details of the mechanisms used to achieve this are lacking in the literature, and the void is even more apparent for ground-test results of mechanism performance. A 1970 NASA report [14] on separation mechanisms acknowledged that several high-profile missions such as Vanguard and Apollo suffered serious setbacks because of malfunctioning separation mechanisms, and it highlighted the need for effective designs and comprehensive testing regimes. The report splits the function of the separation mechanism into two components: the release device and the separation-impulse device. The 1960s technology identified in the report is largely still in use today, which is primarily explosive or pyro-based for the release device and is primarily thruster- or spring-based for the separation-impulse device.

For small-scale satellites the pyro-based release mechanisms have largely been replaced with nonexplosive actuators and shape-memory alloy (SMA) devices [15]. During the ORBCOMM constellation deployment in the 1990s [16,17], a custom separation mechanism integrating nonexplosive-actuator separation nuts and compressions springs was developed to achieve the desired separation conditions. The device was thoroughly tested before launch, but no data are publicly available. At John Hopkins Applied Physics Laboratory, several miniature SMA-based mechanisms were developed in anticipation of the budding microspace market [15]. These mechanisms use SMA technology to accomplish a variety of conventional actuation functions on a small-scale including linear and rotary actuation and three different types of release mechanisms. The devices offer new designs for miniature mechanisms, but no information is available regarding their performance or integration with impulse devices to form a complete separation system designed to meet mission requirements.

At least one commercial-off-the-shelf (COTS) separation mechanism is currently available. It is known as Lightband and is produced by Planetary Systems Corporation [18,19]. It consists of two mating rings with electric motors for releasing and springs for providing impulse. The device has apparently been used by more than 20 spaceflight missions as of 2004 [18] and, despite testing on a microgravity parabolic flight and a study optimizing its design parameters [20], there are little or no data available that quantify its performance. The JC2Sat mission requires a similar nonpyro spring-based separation mechanism, but the presence of solar panels on the mating surface of each satellite calls for a much less invasive design than that of the mating rings.

A unique separation mechanism is under development for the CanX-4 and CanX-5 missions [11], which have speed requirements similar to those of JC2Sat. The distinguishing feature of this mechanism is the use of an adhesive to bond the spacecraft together. The experimental adhesive material loses 90% of its bond strength with the application of a small voltage potential. This type of electrical debonding agent will be tested in space for the first time during the CanX mission and was not considered as a viable option for JC2Sat.

In this paper, a novel ISM is developed that addresses the low-speed and minimally invasive requirements of the JC2Sat mission using a combination of a miniature shape-memory alloy release system and a series of COTS springs. The role of the ISM goes beyond that of most satellite separation systems, in that all the ISM hardware remains attached to the satellites for the entirety of the mission. A ground-testing apparatus using pendulum dummy masses is proposed, and a broad testing regime is undertaken to assess the performance of the ISM. This type of test is similar to specific details of the JC2Sat mission and is presented in Sec. II, followed by a theoretical analysis of the separation dynamics in Sec. III. Details of the ISM, along with its experimental test bed and performance results, are presented in Sec. IV.

II. JC2Sat Formation-Flying Mission

The JC2Sat project is a joint effort between the Canadian Space Agency (CSA) and the Japan Aerospace Exploration Agency (JAXA), which has been proposed to investigate the potential of differential drag for autonomous formation-flying in low Earth orbit (LEO) [4,12]. The mandate is to cooperatively design, build, launch, and operate two 18 kg nanosatellites that will be launched together and separated on orbit. A complementary goal is to use COTS dual-band Global Positioning System receivers to perform centimeter-level relative navigation [21]. In addition, the nanosatellites will serve as a technology demonstration platform for the newly developed miniature far-infrared radiometer (MIRAD) instrument for the purpose of Earth's limb sounding [22].

The differential drag forces are generated by varying the pitch angle of the satellites, each equipped with fixed drag panels, according to closed-loop control commands from the autonomous guidance algorithms [12]. Both the stacked configuration and the nominal formation-flying configurations are shown in Fig. 1. The breadth of formation-flying maneuvers achievable by JC2Sat is limited by the magnitude and direction of the differential drag forces, which are small (due to the extremely low atmospheric density in LEO) and are applicable only in the direction opposing flight. Despite these actuation limitations, previous studies have shown that formation-keeping and a range of formation maneuvers can be achieved using differential drag [3,5,12]. The concept was proposed by Leonard et al. [3] in 1989 and has seen limited use on orbit for formation-keeping by the previously mentioned ORBCOMM constellation [16]. For JC2Sat, formation-keeping and formation maneuvers are planned at several separation distances ranging from 50 m to 5 km.

The two JC2Sat satellites are attached to a common launch-vehicle interface, but they will reach orbit attached only to each other by a series of four cup/cone interfaces that are part of the ISM described in Sec. IV. The four identical ISMs are located along the outer edge of the mating surface: two along the sides and two along the top. One of the side ISMs is visible in Fig. 1; note that there are nonsymmetrical components of each ISM located on both satellites.

Each satellite is three-axis-stabilized using reaction wheels aligned with the pitch axis and magnetorquers along each body axis [23]. The attitude determination is achieved using sun sensors and magnetometers. The attitude control system of only one satellite must be capable of controlling the satellites in the launch or stacked configuration. Initially, the stack will rotate in a power-positive parking mode, but will acquire the desired separation attitude at the designated orbit location for separation. The expected launch orbit is sun-synchronous between 600 and 700 km. From the perspective of differential drag, the formation-flying challenges increase with

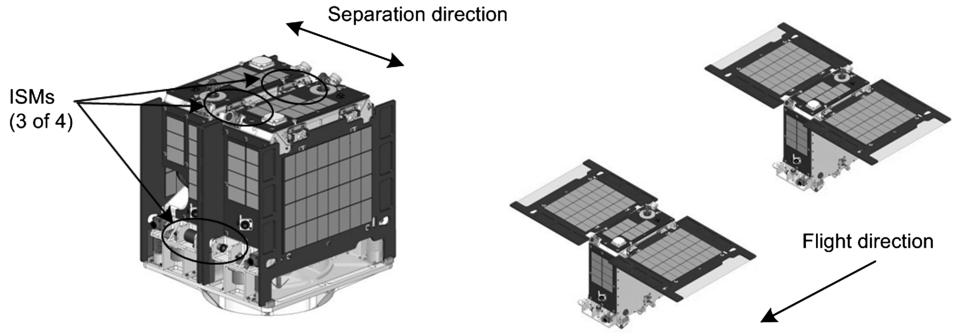

Fig. 1 Illustrations of a) JC2Sat in stacked configuration and b) JC2Sat in nominal orbit-configuration.

altitude, so all analyses in this paper are for 700 km, which is thought of as the worst case. A summary of the basic characteristics of the JC2Sat mission is given in Table 1.

III. Separation Dynamics

The formation-flying mission commences at the moment the satellites separate from their stacked configuration. The objective of intersatellite separation is to effectively detach the two satellites while ensuring that the satellites do not have a collision or drift too far apart. The basic dynamics following separation can be approximated using the well-established Clohessy–Wiltshire (CW) equations [24] in a simplified form, assuming that there is no initial separation between the satellites ($x_0 = y_0 = z_0 = 0$):

$$x(t) = \frac{\dot{x}_0}{n}\sin(nt) - \frac{2\dot{y}_0}{n}\cos(nt) + \frac{2\dot{y}_0}{n} \tag{1}$$

$$y(t) = \frac{4\dot{y}_0}{n}\sin(nt) + \frac{2\dot{x}_0}{n}\cos(nt) - \frac{2\dot{x}_0}{n} - 3\dot{y}_0 t \tag{2}$$

$$z(t) = \frac{\dot{z}_0}{n}\sin(nt) \tag{3}$$

where n is the mean motion of the original circular orbit and x, y, and z are the relative positions between the two satellites in Hill's frame, which is shown in Fig. 2. The initial relative speeds in each axis are related to the separation speed of one satellite, V_0, and the separation angles as follows:

$$\dot{x}_0 = 2V_0 \sin\alpha \tag{4}$$

$$\dot{y}_0 = 2V_0 \cos\alpha \cos\beta \tag{5}$$

$$\dot{z}_0 = 2V_0 \cos\alpha \sin\beta \tag{6}$$

Table 1 Basic characteristics of JC2Sat mission

Item	Specification
Mass	18 kg (each)
Dimensions	35 × 35 × 15 cm (each)
Mission life	1 year
Orbit	LEO (600–700 km), sun-synchronous, circular
Attitude	Three-axis-stabilized, pitch-axis momentum-biased
Communication	Uplink: 9.6 kbps (UHF)
	Downlink: 38.4 kbps (S band)
	Intersatellite link: 9.6 kbps (UHF)
Payloads	MIRAD
	Laser reflector assembly

The separation velocity $\mathbf{V_0}$ is shown in Fig. 2, along with Hill's frame, the local-vertical/local-horizontal coordinate frame attached to the initial circular orbit that is used for the separation analysis. In this frame, $\mathbf{V}_0$ is the velocity of a single spacecraft relative to Hill's frame, and it can be specified by its magnitude V_0, an azimuth angle β, and an elevation angle α.

It should be mentioned that the CW equations describe the unperturbed motion of a body relative to a reference circular orbit, given specific initial conditions. For intersatellite separation, we use the equations to describe the relative motion between two satellites that have the same mass and experience an equal-but-opposite separation force. This is valid, since the CW equations are linear, but it is understood that the linear approximation degrades the further the orbits stray from the original circular orbit. In this context, the separation speed V_0 must be multiplied by a factor of 2 to give the appropriate relative initial velocity between the two satellites. The assumption that no perturbation forces act on the spacecraft is not strictly true when differential drag forces are present; however, the simplified results are pertinent for a preliminary investigation.

An inspection of Eqs. (1–3) reveals several important features of intersatellite separation. A summary of observations follows:

1) The relative motion in the radial direction x is a sinusoid with amplitude and phase that depend on the initial velocity in the x and y directions and on a constant offset that is proportional to the initial along-track velocity $\dot{y}_0$.

2) The relative motion in the along-track direction (y) has a sinusoidal term, a constant offset, and a secular drift. The constant offset is proportional to the initial velocity in the radial direction, while the secular drift is three times the initial separation velocity in the y direction.

3) Motion in the cross-track direction z is purely sinusoidal and has zero crossings every half-orbit (therefore, a pure cross-track separation of $\beta = 90°$ and $\alpha = 0°$ would result in a collision half an orbit after separation).

We are primarily concerned with the motion in the along-track, or y, direction, as it is the only component with a secular term that grows with time. This can be visualized by considering a 2-D simplification of the resulting orbits after separation, as shown in Fig. 3. For simplicity, the azimuth and elevation angles are assumed to be zero: $\beta = \alpha = 0$. From the initial circular orbit, the satellite that is given an initial forward velocity becomes the follower as its semimajor axis increases; conversely, the satellite whose forward velocity is decreased at separation becomes the leader as its semimajor axis decreases. The leader thus has a shorter orbital period, which causes the along-track separation to grow with time. The radial separation, on the other hand, is strictly periodic with a zero mean. If the azimuth angle is not zero, the inclination of the two orbits would also change; however, this would only create a periodic term in the cross-track direction without affecting the planar situation displayed in Fig. 3. If the elevation angle was not zero, the arguments of perigee of the two orbits would no longer be 180 deg apart, and this would impact the periodic terms in the radial and along-track directions.

For the JC2Sat mission, the satellites must maintain a minimum separation distance of 10 m, while the along-track drift must not

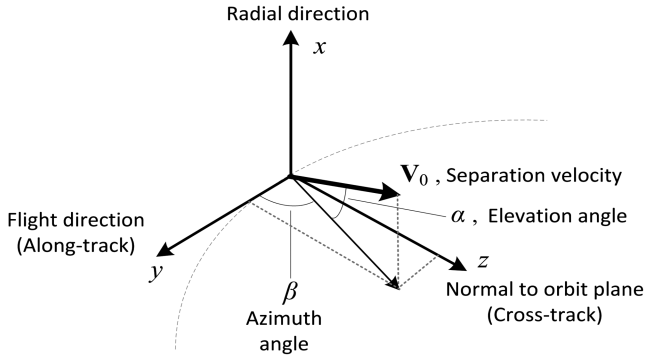

Fig. 2 Hill's frame with separation velocity and angles.

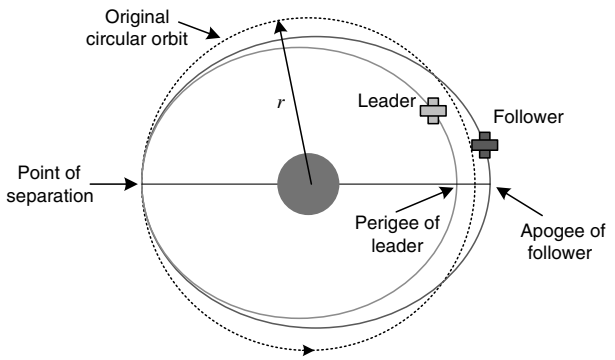

Fig. 3 Elliptical orbits of follower and leader satellites following separation in the along-track direction.

exceed 10 km, and the cross-track amplitude should not become excessive (greater than 1 km). Simplified relationships based on a central-body orbit can be used to analyze these three requirements separately, but when selecting the separation speed and direction, all three requirements must be considered together.

A. Collision Avoidance

The collision-avoidance analysis is performed by solving Eqs. (1–3) with initial conditions provided by Eqs. (4–6) to for a range of separation angles and speeds. Although these equations assume unperturbed orbits, which is not the case if differential drag forces are present, the analysis investigates only the first 1.5 orbits after separation and the accumulative impact of differential drag on such a short time period is negligible. Preliminary analyses for the separation dynamics for JC2Sat indicated that the available differential drag force is only able to overcome very small (less than 1 cm/s) separation speeds in either the radial or the along-track direction. For this reason, the separation velocity must be near the cross-track direction, and thus only the small range of azimuth angles, $80^\circ < \beta < 100^\circ$, and elevation angles, $-5^\circ < \alpha < 5^\circ$, are considered in the current analysis. The outcome with respect to the cross-track motion will be addressed in Sec. III.C.

A contour plot of the results for the minimum separation distance during the first 1.5 orbits (neglecting the first quarter of the initial orbit) for this range of angles is plotted in Fig. 4 for a separation speed of $V_0 = 2$ cm/s. The separation distance varies linearly with the separation speed, so for a speed of $V_0 = 1$ cm/s the separation would be half of that shown in Fig. 4. It is clear that to avoid a situation where the separation is less than 10 m, the azimuth angle should differ by at least 5 deg from the cross-track direction of $\beta = 90^\circ$. It is interesting that the results in Fig. 4 are not symmetric. To ensure an adequate separation distance, it may be necessary to use a small positive elevation angle for azimuth angles less than 90 deg and a slightly negative elevation angle for azimuth angles greater than 90 deg. More detailed simulation results are required to select the final separation angle, but the results presented form a guideline as to the range of angles pose that a serious risk of collision.

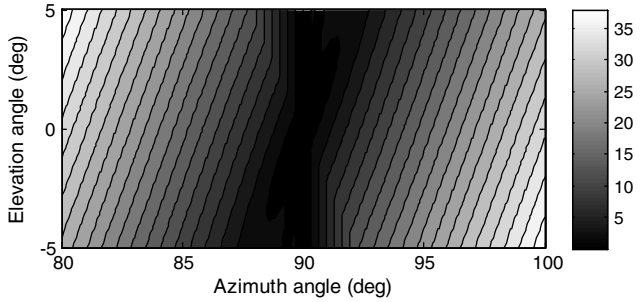

Fig. 4 Minimum separation distance (in meters) encountered during first full orbit with a separation speed of $V_0 = 2$ cm/s for a range of separation angles.

B. Drift-Stop Distance

After the satellites separate they will be detumbled and oriented with their bodies along the flight direction, as shown in Fig. 1. The follower will then be pitched to its maximum pitch angle, which is nominally 60 deg for JC2Sat at an altitude of 700 km. This drift-stop maneuver will be performed until the semimajor axis of the follower is reduced to match that of the leader. To maintain control authority of the formation, preliminary analyses have suggested that the maximum separation distance for the JC2Sat leader/follower should not exceed 10 km.

To predict the behavior of the formation during the drift-stop maneuver, two types of relationships are required: one to determine the difference of the semimajor axis as a result of separation and one for rate of change of the semimajor axis changes when differential drag is present. To find the variation of the semimajor axis, Δa, after separation, the following expression for the satellite's change in speed, Δv, is used:

$$\Delta v = \sqrt{\frac{2\mu}{r} - \frac{\mu}{a}} - \sqrt{\frac{\mu}{r}} \tag{7}$$

where a is the semimajor axis of either satellite after separation, r is the radius of the original circular orbit, and μ is the Earth's gravitational parameter. Rearranging for a gives

$$a = \mu \Big/ \left(\frac{2\mu}{r} - \left(\Delta v + \sqrt{\frac{\mu}{r}} \right)^2 \right) \tag{8}$$

Once a is determined, Δa is found by $\Delta a = a - r$. For a 700 km orbit and a separation velocity of $V_0 = 2$ cm/s, $\beta = 80^\circ$, and $\alpha = 0$, the change in the semimajor axis of one satellite is $\Delta a = 6.55$ m. Since the other satellite will experience the same Δa, but in the opposite direction, the total change in semimajor axis of the follower to complete the drift-stop maneuver is $\Delta a_{\text{tot}} = 13.10$ m.

A simple relationship for the change in semimajor axis over time for a near circular orbit with a constant atmospheric density ρ is given by [25]

$$\Delta a = \frac{-2\pi\rho C_D A a^2 N_{\text{orbits}}}{m} \tag{9}$$

where $C_D = 2.2$ is the drag coefficient, $A = 0.35$ m^2 is the differential frontal area, $m = 18$ kg is the mass of one satellite, and N_{orbits} is the number of orbits. The time taken to stop the along-track drift, in terms of the number of orbits, can be found by rearranging Eq. (9) and solving for N_{orbits}. A standard value of 2.2 for C_D was chosen for JC2Sat, and it is acknowledged that this represents the lower limit of the range expected for a spacecraft with its geometry in LEO. This is acceptable for this analysis, because the differential drag performance will be conservative and because of the large uncertainty associated with atmospheric density, which is addressed next. The atmospheric density, ρ in LEO is difficult to predict, as it

Table 2 Drift-stop results following satellite separation

Altitude, km	V_0, m/s	β, deg	Number of orbits			Along-track drift, m		
			$\rho_{\min}$	ρ_{mean}	$\rho_{\max}$	$\rho_{\min}$	ρ_{mean}	$\rho_{\max}$
700	0.01	80/100	85	18	4	2617	552	102
700	0.01	85/95	43	9	2	660	139	26
700	0.02	80/100	170	36	7	10467	2209	409
700	0.02	85/95	86	18	4	2637	557	103
700	0.04	80/100	339	72	13	41869	8836	1635
700	0.04	85/95	171	36	7	10547	2226	412

depends highly on solar radiation levels. For this analysis, calculations were performed for the minimum, maximum, and mean density values expected at 700 km, which are $\rho_{\min} = 5.74\times 10^{-15}$ kg/m^3, $\rho_{\text{mean}} = 2.72 \times 10^{-14}$ kg/m^3, and $\rho_{\max} = 1.47\times 10^{-13}$ kg/m^3 [26]. Table 2 gives the results for the number of orbits and the along-track drift distance for several separation velocities at each density level. The along-track drift distance was calculated using the initial separation speed and a constant deceleration.

The results clearly show that the drift-stop performance depends heavily on the atmospheric density, which fluctuates in phase with the solar radiation cycle. Predictions are available for the solar activity for the JC2Sat mission, which could potentially be launched in 2013 and have a mission life of 1 year. Figure 5 shows how annual Schatten $F_{10.7}$ solar-flux predictions have changed from 2001 to 2010 [27]. It is clear that the solar predictions have varied drastically over time and that the upcoming cycle will have much less radiation output than has been traditionally observed (represented by the typical curve in Fig. 5 from an empirical polynomial given by Vallado [28]). Although a solar maximum is expected for the potential launch of JC2Sat in 2013, the actual radiation output is expected to be below the mean of a typical solar cycle. Because of the uncertainty in both the solar-flux predictions and the launch date, the results in Table 2 have a more qualitative than quantitative value. For instance, for a speed of 2 cm/s and an azimuth angle of 80 deg, a drift greater than the mean of 2209 m should be expected, but less than the maximum of 10,467 m. This is sufficient for adhering to the 10 km requirement, but if a different launch date was specified where a solar minimum was likely, an azimuth angle closer to 85 deg should be chosen to ensure the required drift stop is met.

A high-fidelity orbit simulator has been developed at CSA to study the formation-flying behavior of JC2Sat. This model employs the 36×36 Goddard Earth model for gravitational effects and includes several other sources of perturbations such as sun and moon gravity perturbations, as well as aerodynamic drag and lift forces generated using a Jacchia 70 atmospheric model [29]. To confirm the drift-stop results in Table 2, simulations were run where the follower satellite is pitched immediately after separation and drift stop is achieved once the relative along-track drift between the two spacecraft becomes zero (an oscillatory component may still be present). For a launch date of January 2013, using the 2010 Schatten solar-flux prediction, a drift-stop distance of approximately 4000 m was observed for a speed of 2 cm/s and an azimuth angle of 80 deg. This appears to corresponds to the results suggested in Table 2 for the atmospheric density slightly less than the mean. Using the simulator it was observed that the drift-stop distance varied depending on the argument of latitude at which separation occurred. Figure 6 shows a plot of a series of simulation results at 30 deg increments over the full range of argument of latitude. An elliptic shape was fit to the results, indicating that near the poles the drift-stop distance (4450 m) is greater than near the equatorial plane (3750 m).

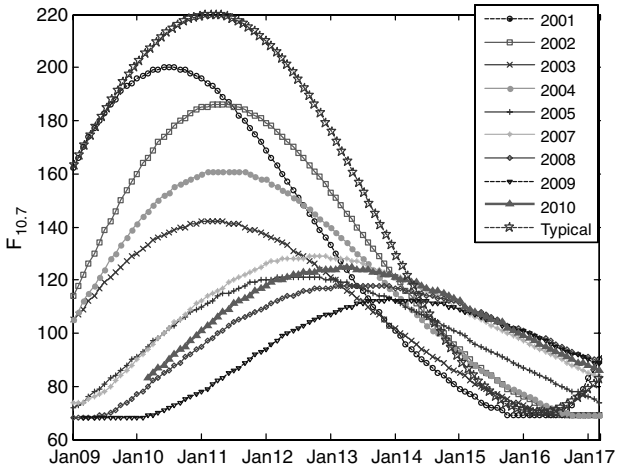

Fig. 5 Evolution of Schatten solar-flux predictions made between 2001 and 2010 [27,28].

C. Cross-Track Drift

It is important to understand the cross-track behavior of the formation, because the differential drag technique has little or no ability to provide control actuation in this direction. Because of the nonzero azimuth angle during separation there will be sinusoidal relative motion in the cross-track direction, whose amplitude depends on the component of the separation velocity in the cross-track or z direction [Eq. (6)]. This cross-track motion is the result of differences in the inclination i and right ascension of the ascending node (RAAN), Ω, of the leader and follower orbits following separation. If separation occurred at the equator, only the inclination would be different, but if it occurred over the poles, only the RAAN would be different. For the JC2Sat mission, cross-track drift of up to 1 km is deemed acceptable.

It is well-known that the J_2 orbit-perturbation causes ascending-node precession at a rate that depends on the inclination angle of the orbit. If separation does not occur over the poles (the current plan is to

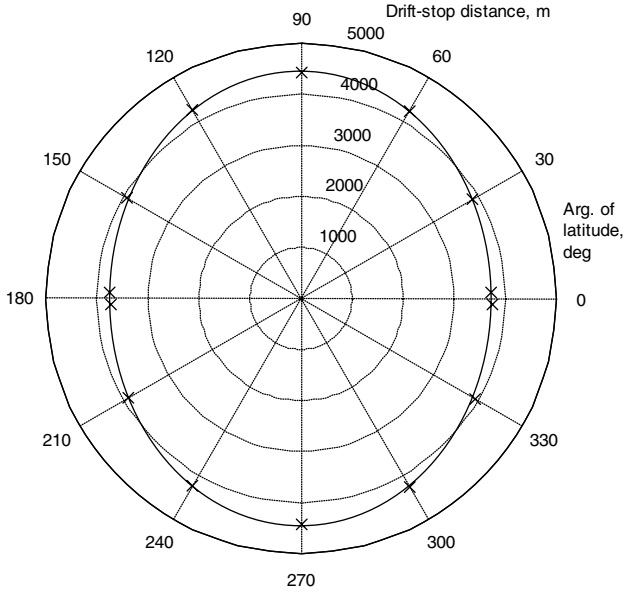

Fig. 6 Distribution of drift-stop distances over the full range of argument of latitude.

separate JC2Sat over a Toronto ground station at 43°N), the two satellites will have slightly different inclination angles and, hence, slightly different ascending-node precession rates. The precession rate $\dot{\Omega}$ can be calculated using the following relationship [30]:

$$\dot{\Omega} = \frac{-3J_2R_E^2 n}{2p^2}\cos i \tag{10}$$

where

$$p = a_0(1 - e^2) \tag{11}$$

The differential precession rate between the two satellites is

$$\Delta\dot{\Omega} = \frac{-3J_2R_E^2 n}{2p^2}(\cos i_L - \cos i_F) \tag{12}$$

To use Eq. (12) the inclination angle of the satellites (leader and follower) after separation must be known. The inclination change resulting from separation, i_s, can be calculated using the separation velocity vectors and spherical trigonometry relationships, which results in the following equation [30]:

$$\cos i_s = \cos i_0 \cos\theta - \sin i_0 \sin\theta \cos u_0 \tag{13}$$

where θ is the angle of the plane change during separation, i_0 is the inclination of the original orbit, and u_0 is the argument of the latitude. Equation (13) is also used to estimate the initial amplitude of the cross-track relative motion, z_{A_0}. The growth of the cross-track amplitude, $\dot{z}_A$, is related to the ascending-node precession rate by

$$\dot{z}_A = 2a \sin\left(\frac{\dot{\Omega}}{2}\right) \tag{14}$$

The results for the initial amplitude of cross-track motion, z_{A_0}, and cross-track drift, $\dot{z}_A$, are given in Table 3. The results indicate that the amplitude of the cross-track motion will exceed the desired 1 km limit after 1 year for separation speeds above 1 cm/s. It has been observed in high-fidelity simulations that separating during a descending pass slightly reduces the cross-track drift, so it is possible that a separation speed of 2 cm/s will meet the cross-track requirement. In any case, the 1 km cross-track limit is a soft requirement that may be slightly relaxed if necessary.

D. Separation Dynamics Discussion

The most important performance indicator of the separation dynamics is the along-track drift. A simplified analytic expression over a range of atmospheric density values provided an approximation of the drift-stop distance using predicted solar-flux levels as a guide. Simulation results using a nonlinear model with several sources of perturbations provided results that fall within the approximated range. A more comprehensive and sophisticated analysis of the drift-stop performance was performed independently by Hamel et al. [31] using Monte Carlo techniques to include the statistical variability in numerous design and environmental parameters. The approximations obtained in Sec. III are consistent with the Monte Carlo results [32]; however, it is clear that the high-fidelity simulation and the Monte Carlo analyses provide a more reliable and comprehensive picture of the drift-stop behavior by taking into account higher-order dynamics and parameter uncertainty.

Table 3 Cross-track motion caused by intersatellite separation

Altitude, km	V_0, m/s	β, deg	z_{A_0}, m	$\dot{z}_A$ m/day	$\dot{z}_A$ m/year
700	0.01	80/100	18.6	1.63	612
700	0.01	85/95	18.8	1.64	619
700	0.02	80/100	37.2	3.25	1224
700	0.02	85/95	37.6	3.29	1238
700	0.04	80/100	74.4	6.49	2448
700	0.04	85/95	75.2	6.58	2476

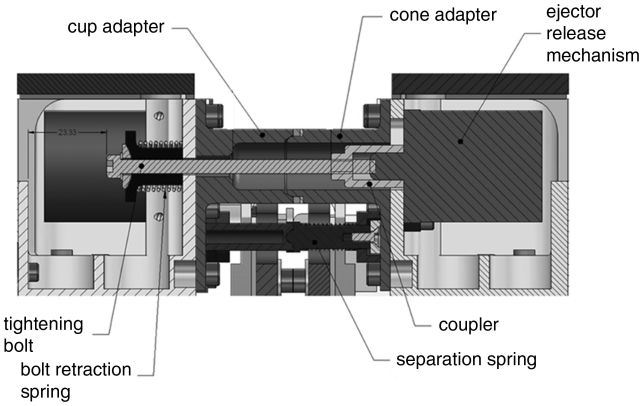

Fig. 7 CAD model of ISM cross section; the ERM is loaded and the separation and bolt-retraction springs are compressed.

The results in Fig. 6 show that because of gravity perturbations, the precise location on orbit where separation occurs can influence the drift-stop distance. If separation occurs near the equatorial plane, the drift-stop distance is minimized. This contradicts the interest of the cross-track drift, which was found to be minimized when separating near the poles. The current plan for JC2Sat is to separate over its ground station located in Toronto (43°N); however, this decision could be revisited once the final orbit is known, depending on whether the predicted along-track or cross-track behavior is approaching the limits imposed by the mission requirements.

Although a precise separation velocity or location is not specified in this paper, the collision avoidance, drift stop, and cross-track results serve as a coarse guideline that suggests that the azimuth angle should be at least 5 deg away from pure cross-track separation at $\beta = 90°$, and the speed should be no greater than $V_0 = 2$ cm/s. Designing and testing a separation mechanism that will ensure a separation speed less than 2 cm/s is a major challenge and will be discussed in the next section.

IV. Intersatellite Separation Mechanism

The satellites initially reach orbit together in a stacked configuration, attached by four ISMs. Before separation two of the four ISMs are released, and at the desired moment the remaining two ISMs are released and separation occurs. The two-stage ISM release is done to limit the separation speed and simplify the synchronization circuitry. Although only two ISMs are activated to achieve the final separation, it is still necessary to use four ISMs to rigidly attach the satellites ensure that the structural integrity of the stacked satellites is maintained during launch.

The ISM is composed of several components, which can be seen in the cross section of a CAD model in Fig. 7. A photograph of a prototype ISM is shown in Fig. 8 (geometry is reversed compared with Fig. 7). The centerpiece of the ISM is the ejector release mechanism (ERM), which is an electronically triggered SMA device manufactured by Tini Aerospace (part number ERM-500). Before launch, the satellites are rigidly attached at the ISM's cup/cone adapters by applying sufficient tension to the tightening bolt, which is coupled from one satellite to the ERM on the opposing satellite. The following steps describe the sequence of events in the separation process:

1) When the ERM receives an appropriate voltage input, it releases and ejects the coupler.

2) The coupler and the tightening bolt are also pulled away from the ERM by the bolt-retraction spring located on the satellite opposite to the ERM.

a) b) c)

Fig. 8 Photographs of a) ISM showing bolt-retraction spring and separation spring, b) Tini ERM-500 ejector release mechanism (not loaded), and c) microswitch.

3) The momentum of the coupler leaving one satellite body is transferred to the other satellite causing the satellites to move in opposing directions.

4) An additional separation force is applied to each satellite by the separation spring and microswitch.

Although only two distinct springs are identified in Fig. 7, there are potentially four spring elements in each ISM that contribute to the separation: the ejector spring (E) inside the ERM, the bolt-retraction spring (BR), the separation spring (SS), and the microswitch spring (MS). The microswitch is a simple contact switch that detects if/when the actual separation occurs and is shown in Fig. 8. The stiffness, compression distance, and energy stored for each spring is given in Table 4. The ejector and the bolt-retraction springs clearly store the most energy, but because both of those springs act on the retraction bolt, which is much lighter than the satellites, only a small fraction (less than 1%) of their potential energy is converted into kinetic energy of the satellites. On the other hand, both the separation spring and the microswitch act directly on both bodies, so neglecting losses, all their stored energy is transferred to the separation velocities of the satellites.

A. Experimental Apparatus

The performance of the ISM was tested at JAXA Tsukuba to evaluate its design and predict its behavior in space. The tests involved engaging the ISM while two 17 kg satellite dummy masses were individually suspended by vertical wires. A schematic and a photograph of the test setup are provided in Figs. 9 and 10, respectively. From Fig. 10 it is apparent that only two ERM units are involved in the tests at the active ISM locations. This simplifies the tests and accurately simulates the conditions of the final separation on orbit. The position at three different locations on the outside surface of each body were measured using laser ranging sensors. The slope of the average of the three position measurements over time was used to estimate the separation speed for each satellite. An estimate of the tipoff rate is also possible with this sensor arrangement; however, it was not considered in this study.

The pendulum support for each body is intended to minimize the gravitational effects on the separation motion. This configuration is similar to a cold-gas thruster test bed developed by Lugini and Romano [33]. Initially, the component of gravity is strictly vertical and, as such, does not impede the horizontal motion of the bodies. However, once separation occurs the support wire becomes angled and its tension will have a component in the horizontal direction. To assess gravity's role in the pendulum motion of each body, the simple linear pendulum equation subject to a forcing function $F(t)$ can be used:

Table 4 Details of ISM spring elements

Spring	Stiffness, N/m	Compression, m	Energy per spring, J
E	4553	0.00635	0.0918
BR	360	0.0315	0.1786
SS	98	0.001	0.00015
MS	714	0.003	0.00321

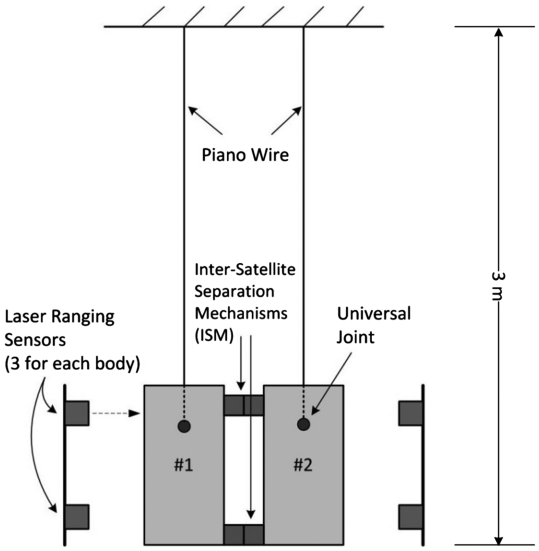

Fig. 9 Schematic of ISM test apparatus.

$$m\ddot{d} - mg\frac{d}{l} = F(t) \tag{15}$$

where d is the horizontal distance traveled by one body, and l is the length of the support wire. Solving this differential equation by assuming that the body is subject to an initial impulse gives the predicted motion of the test article. This result can be compared with the results mimicking conditions in space ($g = 0$), to give an idea as to how well the pendulum test can be expected to represent spacelike conditions. Figure 11 shows the position and velocity for a typical separation with and without gravity. As expected, the effects of gravity become more distinguished with time; however, it is clear that if the velocity can be measured shortly after the initial impulse, the measurement will closely match what can be expected on orbit.

B. Test Results

A plot of the average position of the two dummy masses, along with the input voltage to the ERM, is given in Fig. 12 for one particular test case. Pendulum motion with a 1.5 cm amplitude and period of 1.7 s is observed. When estimating the slope of the displacement curve to obtain the speed, it is important to use data as soon as possible after separation so that the gravitational effects are minimal. Figure 13 shows a close-up of the data for the time interval between 1.66 and 1.74 s. This interval, chosen as the start of the approximately linear region following the initial impulse, was used to estimate the separation speed. A summary of the test results is given in Table 5. For each test scenario, between two and four trials were performed, and Table 5 includes the average speeds over the trials, as well as the standard deviation.

The speed for test 1 was approximately four times higher than expected, as the ISMs were designed to deliver a separation speed of

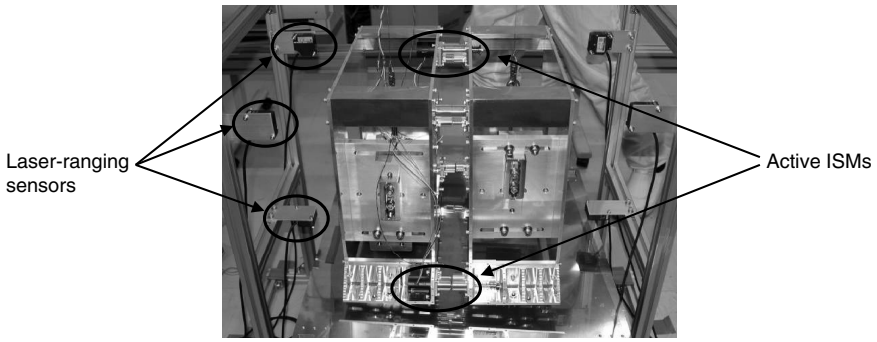

Fig. 10 Photograph of test setup at JAXA showing dummy masses, ejectors, and laser ranging.

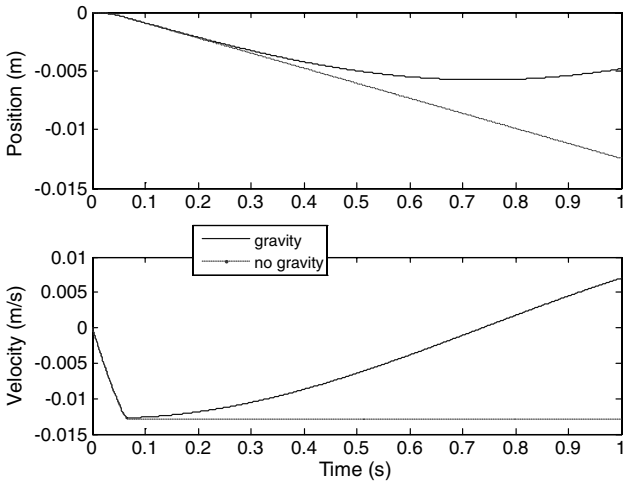

Fig. 11 Simulated results for pendulum tests with and without gravity.

1 cm/s. A thorough analysis of the separation mechanism suggested that only part of the unexpected additional velocity could be from the ISM springs. It was thought that a significant part of the extra speed was due to neglected strain energy that is stored in the structure when the satellites are fixed together by applying a torque to the tightening bolt that mates with the threads in the coupler (Fig. 7). The preload torque on the bolt for test 1 was 1.2 Nm, so to test this hypothesis the torque was reduced in half to 0.6 Nm for test 2. As anticipated, a lower separation speed was observed. It is expected that the speed could be decreased further if the preload torque is reduced below 0.6 Nm, but this is not a realistic option, as a semirigid connection between the satellites is necessary for enduring launch loads.

An alternative approach for achieving low separation speeds, termed soft release, was proposed and tested. This technique involves constraining the bodies during activation of all four ISMs using a thin wire wrapped around the outside of both bodies. With the ISM attachment points released, the final separation only occurs after the wire is severed by the application of a moderate heat source, similar to the CubeSat separation mechanism in [34]. The test configuration and the heat-based wire cutter are shown in Fig. 14. Tests 3 and 4 in Table 5 used the soft-release approach. For test 3, the only springs acting on the bodies were the separation springs, and for test 4 the microswitches were also used. From these results it is obvious that low separation speeds (less than 2 cm/s) are achievable. It is also clear that the microswitches provide a significant contribution to the separation energy.

For the soft-release tests, it is fruitful to compare the results with speeds predicted using simple conservation of energy equations. For test 3, if the stored energy in the springs (4×0.00015 J) is converted entirely into kinetic energy of the bodies, $\mathrm{KE} = mV_0^2/2$, the predicted speed V_0 is 0.59 cm/s. This corresponds precisely with that measured for satellite 2 and is slightly higher than the speed of satellite 1. For test 4, the predicted speed resulting from the stored energy in the springs and microswitches is $V_0 = 2.81$ cm/s. This is higher than the measured values, indicating that either the stored energy in the switches is overestimated and/or there are energy losses. Because of the energy imparted by the switches, it could be desirable to eliminate the separation springs and rely only on the switches; however, this is not considered at this moment, because noncontact switches may be chosen in the final design, and the repeatability of the switch stiffness does not appear to be as good as with the helical separation springs.

There are several details regarding the implementation of the soft-release method for the JC2Sat mission that must be addressed before the detailed design process is complete. These include the need for redundancy in case the wire is severed during launch, the amount of tension applied to the wire to ensure that the two satellites are fixed together properly after the ISMs are released, and the reliability of the wire cutter. The purpose of this paper is to demonstrate that low-speed separation can be achieved using this technology.

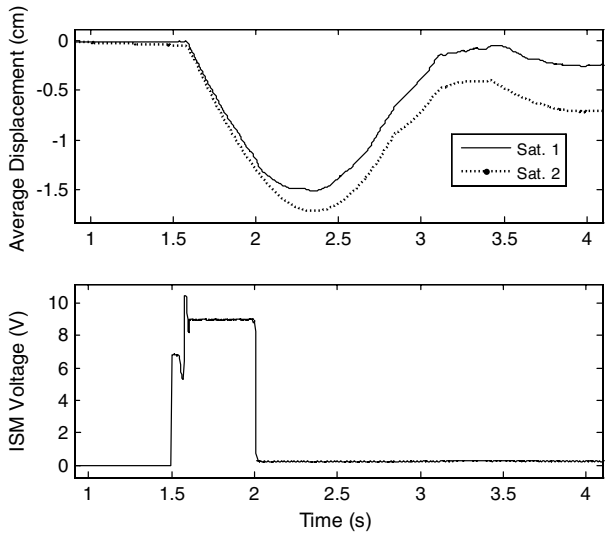

Fig. 12 Average displacement and voltage for test 1.

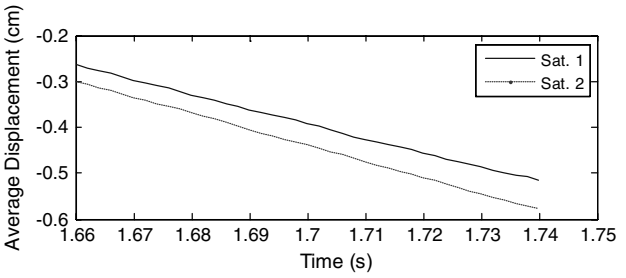

Fig. 13 Average displacement results used for slope estimation for the time interval between 1.66 s and 1.74 s of test 1.

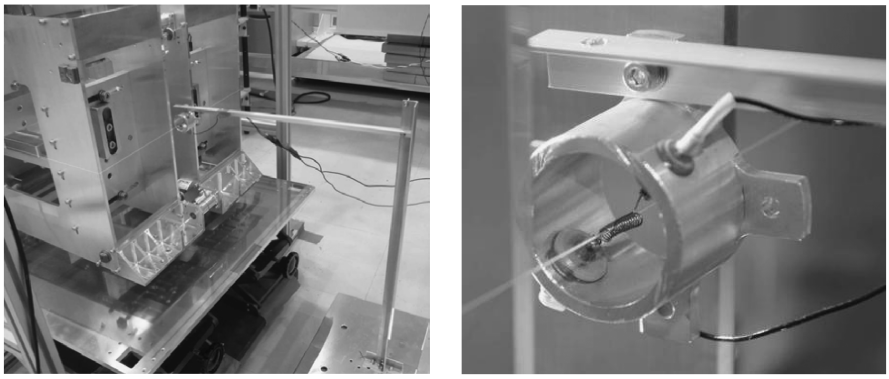

a) b)

Fig. 14 Photographs of a) test setup for soft-release test and b) close-up of soft-release wire cutter.

Table 5 Summary of ISM test results

Test number	Release type	Springs	Preload, Nm	V_1, cm/s	σ_{V1}, cm/s	V_2, cm/s	σ_{V2}, cm/s
1	ISM	E, BR, SS, MS	1.2	4.10	0.77	4.07	0.50
2	ISM	E, BR, SS, MS	0.6	2.84	0.25	3.29	0.23
3	Soft	SS	N/A	0.47	0.31	0.59	0.09
4	Soft	SS, MS	N/A	1.82	0.04	1.98	0.06

V. Conclusions

Intersatellite separation is a critical phase for formation-flying missions involving small-scale spacecraft. This is especially true for the JC2Sat mission, due to the limited control actuation of differential drag. Straightforward analytical expressions can be used to study the separation dynamics in terms of collision avoidance, drift-stop performance, and cross-track drift. The drift-stop behavior is highly dependent on the atmospheric density, which is extremely difficult to predict. Instead of attempting to accurately model the atmosphere, a range of densities that depend on the solar cycle were used to provide insight into what the approximate drift-stop distance would be for a certain launch date. From the results it appears that the mission requirement for drift-stop distance of less than 10 km shall be met. The conflicting requirements of all aspects of separation (namely, collision avoidance, drift-stop distance, and cross-track drift) must be carefully considered when finalizing the separation conditions for a specific orbit. To meet JC2Sat's requirements at a 700 km orbit, the separation velocity should not be more than 2 cm/s and should be directed at an angle at least 5 deg off of the cross-track direction. The location on-orbit where separation occurs was also shown to affect the drift-stop distance and the cross-track drift, indicating that it must also be considered when finalizing the mission plan.

The mechanism designed to facilitate separation in-orbit (the ISM) was tested, and the separation speeds were higher than expected. This is largely due to unaccounted-for strain energy stored in the satellite structure during the attachment process, demonstrating a significant challenge that exists for small-satellite separation mechanisms; they must be able to absorb considerable energy during launch followed by releasing the spacecraft on orbit with minimal energy transfer. A simple technique, involving a thin wire to constrain the satellites while the stored energy is released during ISM activation, was tested and shown to reduce the separation speed to below the 2 cm/s threshold.

Acknowledgments

The authors would like to thank Oikawa of W. E. L. Research in Japan, Takeya of Advanced Engineering Services of Japan, and Kawashima at the Japan Aerospace Exploration Agency for their contributions to the experimental testing.

References

[1] Fleeter, R., *The Logic of Microspace*, Microcosm Press, El Segundo, CA, and Kluwer Academic, Boston, 2000.

[2] Kapila, V., Sparks, A. G., Buffington, J. M., and Yan, Q., "Spacecraft Formation Flying: Dynamics and Control," *Journal of Guidance, Control, and Dynamics*, Vol. 23, No. 3, 2000, pp. 561–564. doi:10.2514/2.4567

[3] Leonard, C. L., Hollister, W. M., and Bergmann, E. V., "Orbital Formation-Keeping with Differential Drag," *Journal of Guidance, Control, and Dynamics*, Vol. 12, No. 1, 1989, pp. 108–113. doi:10.2514/3.20374

[4] Kumar, B. S., Ng, A., Yoshihara, K., and De Ruiter, A., "Differential Drag as a Means of Spacecraft Control," *Proceedings of the 2007 IEEE Aerospace Conference*, IEEE, Piscataway, NJ, March 2007, pp. 1–9.

[5] Bevilacqua, R., and Romano, M., "Rendezvous Maneuvers of Multiple Spacecraft Using Differential Drag Under J_2 Perturbation," *Journal of Guidance, Control, and Dynamics*, Vol. 31, No. 6, 2008, pp. 1595–1607. doi:10.2514/1.36362

[6] Kong, E. M. C., Kwon, D. W., Schweighart, S. A., Elias, L. M., Sedwick, R. J., and Miller, D. W., "Electromagnetic Formation Flight for Multi-Satellite Arrays," *Journal of Spacecraft and Rockets*, Vol. 41, No. 4, 2004, pp. 659–666. doi:10.2514/1.2172

[7] Li, H., and Williams, T., "Reconfiguration of Sun-Earth Libration Point Formations Using Solar Radiation Pressure," *Journal of Spacecraft and Rockets*, Vol. 43, No. 6, 2006, pp. 1328–1339. doi:10.2514/1.16348

[8] Williams, T., and Wang, Z.-S., "Potential Uses of Solar Radiation Pressure in Satellite Formation Flight," *International Journal of Robust and Nonlinear Control*, Vol. 12, Nos. 2–3, 2002, pp. 162–183. doi:10.1002/rnc.681

[9] Persson, A., Veldman, S., and Bodin, P., "PRISMA—A Formation Flying Project in Implementation Phase," *Acta Astronautica*, Vol. 65, 2009, pp. 1360–1374. doi:10.1016/j.actaastro.2009.03.067

[10] Orr, N. G., Eyer, J. K., Larouche, B. P., and Zee, R. E., "Precision Formation Flight: The CanX-4 and CanX-5 Dual Nanosatellite Mission," 21st AIAA/USU Conference on Small Satellites, Paper SSC07-V1-2Aug. 2007.

[11] Larouche, B. P., Bonin, G., Grant, C., and Zee, R. E., "The Intersatellite Separation System: A Lightweight, Low-Power Deployment Mechanism for Formation Flying Nanosatellites," *Proceedings of the 59th International Astronautical Congress*, IAC Paper 08-B4.6.B8, Glasgow, Scotland, U.K., Oct. 2008, pp. 4275–4284.

[12] Kumar, B. S., and Ng, A., "A Bang-Bang Control Approach to Maneuver Spacecraft in a Formation with Differential Drag," Proceedings of the AIAA Guidance, Navigation and Control Conference and Exhibit, AIAA Paper 2008-6469, Honolulu, Aug. 2008.

[13] Sabol, C., Burns, R., and McLaughlin, C. A., "Satellite Formation Flying Design and Evolution," *Journal of Spacecraft and Rockets*, Vol. 38, No. 2, 2001, pp. 270–278. doi:10.2514/2.3681

[14] Mitchell, D. H., "Flight Separation Mechanisms," NASA Langley Research Center, Rept. NASA-SP-8056NASA, Hampton, VA, 1970.

[15] Willey, C. E., Huettl, B., Dowen, D., and Hill, S. W., "Miniature Mechanisms Tool Kit for Micro Spacecraft," *John Hopkins APL Technical Digest*, Vol. 22, No. 2, April 2001, pp. 115–119.

[16] Maclay, T., and Tuttle, C., "Satellite Station-Keeping of the ORBCOMM Constellation Via Active Control of Atmospheric Drag: Operations, Constraints, and Performance," *Advances in the Astronautical Sciences*, Vol. 120, Part 1, 2005, pp. 763–773; also American Astronautical Society Paper 05-152.

[17] Robinson, A., Courtney, C., and Moran, T., "Non-Explosive Actuation for the ORBCOMM Satellite," *Proceedings of the 29th Aerospace Mechanisms Symposium*, 1995.

[18] Holemans, W., "The Lightband as Enabling Technology for Responsive Space," *2nd AIAA Responsive Space Conference*, RS2-2004-7005, 2004.

[19] Holemans, W., "Lessons Learned Developing Separation Systems for Small Satellites," 20th AIAA/USU Conference on Small Satellites, Paper SSC06-IX-7, Aug. 2006.

[20] Tayefi, M., and Ebrahimi, M., "Design and Analysis of Separations Systems Based on an Optimization Approach," 49th AIAA Aerospace Sciences Meeting, AIAA Paper 2009-0436, Orlando, FL, Jan. 2009.

[21] de Ruiter, A., Lee, J., and Ng, A., "Orbit Determination and Relative Position Techniques for JC2Sat-FF," *Proceedings of the 3rd International Symposium on Formation Flying, Mission and Technologies*, SP 654, ESA, Noordwijk, The Netherlands, Apr. 2008.

[22] Ngo Phong, L., and Châteauneuf, F., "Nanosatellite Distributed far Infrared Radiometers," *Proceedings of SPIE*, Vol. 7208, Jan. 2009, Paper 72080L. doi:10.1117/12.814248

[23] de Ruiter, A., Lee. J., Ng. A., Lambert, C., Hamel, J.-F., de Lafontaine, and Shankar, B., "Overview of Japan Canada Joint Collaboration Satellites (JC2Sat) GNC Challenges and Design," AIAA Guidance, Navigation and Control Conference and Exhibit, AIAA Paper 2010-7765, Toronto, Aug. 2010.

[24] Clohessy, W. H., and Wiltshire, R. S., "Terminal Guidance Systems for Satellite Rendezvous," *Journal of the Aerospace Sciences*, Vol. 27, No. 9, 1960, pp. 653–658.

[25] Boden, D. G., "Introduction to Astrodynamics," *Space Mission Analysis and Design*, edited by J. R. Wertz, and W. J. Larson, 3rd ed., Microcosm Press, El Segundo, CA, and Kluwer Academic, Boston, 1999, p. 149.

[26] Wertz, J. R., and Larson, W. J. (eds.), *Space Mission Analysis and Design*, 3rd ed., Microcosm Press, El Segundo, CA, and Kluwer Academic, Boston, 1999.

[27] STK, Satellite Tool Kit, Software Package, Analytical Graphics Inc., Exton, PA, 2010.

[28] Vallado, D., *Fundamentals of Astrodynamics and Applications*, 3rd ed., Microcosm Press, El Segundo, CA, and Kluwer Academic, Boston, 2007.

[29] Roberts, C. E. Jr., "An Analytic Model for Upper Atmosphere Densities Based Upon Jacchia's 1970 Models," *Celestial Mechanics*, Vol. 4, 1971, pp. 368–377. doi:10.1007/BF01231398

[30] Chobotov, V. A., *Orbital Mechanics*, AIAA Education Series, AIAA, Washington, D.C., 1991.

[31] Hamel, J.-F., de Lafontaine, J., Lambert, C., and Ng, A., "Performance Assessment of the Drag-Based Formation Control for the JC2Sat Mission," AIAA Guidance, Navigation and Control Conference and Exhibit, AIAA Paper 2010-7711, Toronto, Aug. 2010.

[32] Lambert, C., Vincent, P., Ng, A., Nakamura, Y., Horiguchi, H., Hamel, J.-F., et al., "Inter-Satellite Separation Analysis of JC2Sat Formation Flying Mission," AIAA/AAS Astrodynamics Specialist Conference, AIAA Paper 2010-7957, Toronto, Aug. 2010.

[33] Lugini, C., and Romano, M., "A Ballistic-Pendulum Test Stand to Characterize Small Cold-Gas Thruster Nozzles," *Acta Astronautica*, Vol. 64, 2009, pp. 615–625. doi:10.1016/j.actaastro.2008.11.001

[34] Fujiwara, K., Omagari, K., Iljic, T., Masumoto, S., Konda, Y., Yamanaka, T., et al., "Tokyo Tech Nano-Satellite Cute-1.7 + APD Flight Operation Results and the Succeeding Satellite," *Proceedings of the 57th International Astronautical Congress*, IAC Paper 06-B5.3.02, Valencia, Spain, Oct. 2006.

C. McLaughlin
Associate Editor